Fermi National Accelerator Laboratory

FERMILAB-Conf-97/099-E
CDF

The CDF SVX II Upgrade for the Tevatron Run II

Daniela Bortoletto
For the CDF Collaboration

Physics Department, Purdue University
West Lafayette, Indiana

Fermi National Accelerator Laboratory
P.O. Box 500, Batavia, Illinois 60510

April 1997

Published Proceedings of *VERTEX96, 5th International Workshop on Vertex Detectors*,
Chia, Italy, June 16-21, 1996

Disclaimer

Distribution

THE CDF SVX II UPGRADE FOR THE TEVATRON RUN II

Daniela Bortoletto*
representing the CDF collaboration
Physics Department
Purdue University
West Lafayette, Indiana
USA

Abstract

A microstrip silicon detector SVX II has been proposed for the upgrade of CDF to be installed in 1999 for Run II of the Tevatron. Three barrels of five layers of double-sided silicon microstrip detectors will cover the interaction region. A description of the project status will be presented. Emphasis will be given to the R&D program for silicon sensors which includes capacitance minimization, the study of coupling capacitor integrity, the operation of the detectors in conjunction with the SVXH and SVX2 readout chips in two beam tests and the determination of the detectors performance deterioration due to radiation damage.

*corresponding author 1396 Physics Department, Purdue University, 47907 West Lafayette, IN, USA, *daniela@fnald.fnal.gov*.

1 Introduction

The SVX II detector is an integral part of the CDF upgrade for run II of the Tevatron. During this run, CDF is expected to collect about 2 fb^{-1} of data at $\sqrt{s}$ of 2 TeV. The tenfold statistical increase will allow precision studies of the top quark production and decays. It is also likely to provide a measurement of CP violation in the B system. The detector design is driven by the Run II (Run III) high luminosity of 1×10^{32} cm^{-2} sec^{-1} (1×10^{32} cm^{-2} sec^{-1}), the Tevatron short bunch spacing of 396 ns (132 ns), and by the physics requirement of b decay vertex identification within collimated high P_t jets.

SVXII, the next generation vertex detector, is comprised of three cylindrical barrels which cover $\approx 2.5\ \sigma$ of the interaction region providing track information to pseudo-rapidity $|\eta| < 2$. Five layers of double sided silicon sensors supply r-ϕ as well as 3 r-z and 2 small angle stereo measurements. The result should provide good pattern recognition and 3-d vertex reconstruction with an impact parameter resolution $\sigma_\phi < 30\mu$m and $\sigma_z < 60\mu$m for central high momentum tracks.

The 405,504 channels in the system are connected to radiation hard SVX 3 chips [1] mounted on electrical hybrids glued to the surface of the silicon sensors. Each chip has 128 channels holding a charge sensitive amplifier and a 42 cell pipeline with simultaneous digitization and readout of data allowing a 50 kHz Level 1 trigger rate with minimal deadtime. A highly parallel fiber data aquisition system enables the readout of the entire detector in $\approx 10\ \mu$s and the operation of the Silicon Vertex Tracker (SVT), a large impact parameter level 2 trigger. The ability to trigger on b displaced vertices is crucial for the measurement of CP violation in the $B \rightarrow \pi^+\pi^-$ channel.

Here we briefly discuss the mechanical design and we present recent results on the silicon sensor development.

2 Mechanical design

The SVX II detector is divided into three 29 cm long barrels segmented in 12 $r-\phi$ wedges, each with five layers of silicon. Within each barrel, the silicon ladders are mounted between two precision-machined beryllium bulkheads which also carry the water cooling channels for the readout electronics. Figure 1 shows a drawing of the SVX II bulkhead. The radial locations of the layers are given in Table 1.

Detector Parameters	SVX II
Readout coordinates	r-ϕ; r-z
Number of barrels	3
Number of layers per barrel	5
Number of wedges per barrel	12
Ladder length	29.0 cm
Combined barrel length	87.0 cm
Layer geometry	staggered radii
Radius innermost layer	2.44 cm
Radius outermost layer	10.6 cm
r-ϕ readout pitch	60;62;60;60;65 mm
r-z readout pitch	141;125.5;60;141;65 mm
Length of readout channel (r-ϕ)	16.0 cm
r-ϕ readout chips per ladder	4;6;10;12;14
r-z readout chips per ladder	4;6;10;8;14
r-ϕ readout channels	211,968
r-z readout channels	193,536
Total number of channels	405,504
Total number of readout chips	3168
Total number of detectors	720
Total number of ladders	180

Table 1: Parameters of the 5-layer SVX II detector.

In order to allow possible replacement of the inner two layers due to radiation damage, the bulkhead will have the inner two layers separated from the outer three layers. The inner section will be

attached to the outer section with pins and splice plates that lie along the radial spokes. We expect repeatable location of the two parts within 3 microns.

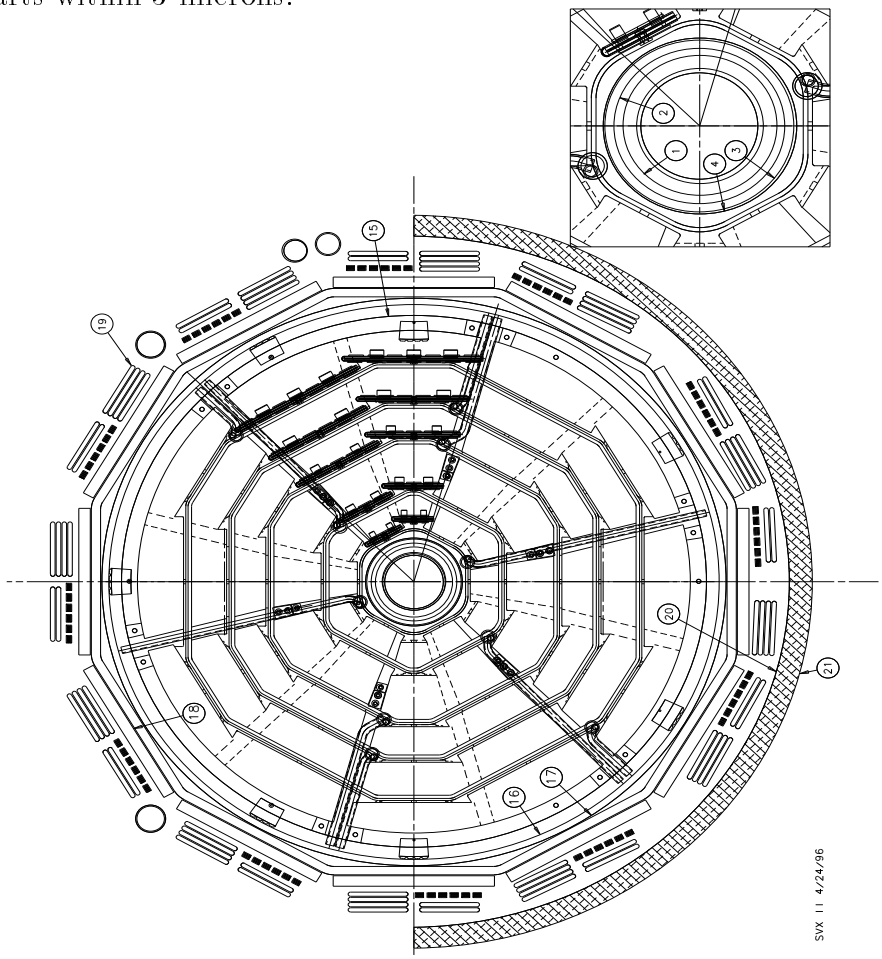

Figure 1: The SVX II bulkhead design

Shown in Figure 2 is a perspective view of a Layer 0 ladder. A notch on the ladder end is used during ladder construction and will precisely locate ladders relative to the support structure. The ϕ-side of the sensor is on the top of the ladder with the SVX3 chips directly opposite the cooling channel. The z-side SVX3 chips are located inboard of the cooling channel on the underside of the ladder. To reduce the dead region between barrels, the hybrid is glued onto

the silicon sensor surface.

The silicon sensor layout is optimized to allow good secondary vertex reconstruction and pattern recognition, key elements for b-tagging in a dense jet environment. This leads to the first, second and fourth layers (Layers 0, 1 and 3) having longitudinal p^+ implant strips on the p-side measuring the $r-\phi$ coordinates in the plane perpendicular to the beam axis. The $r-z$ coordinates, along the beam axis, are measured by orthogonal n^+ strips on the n-side. Both sets of strips are read out from the end of the sensors. For the r-z coordinates this requires an additional layer of strips running longitudinally and contacting the lateral r-z strips through a 5 μm insulating layer of SiO_2 by means of small "vias". This is referred to as a double-metal layer technology.

The Layer 2 and Layer 4 sensors utilize "small angle stereo" for the strip layout. The design of these sensors takes advantage of the six inch wafer technology. Such large wafers can host both a Layer 2 and a Layer 4 detector, reducing the mask fabrication and processing costs.

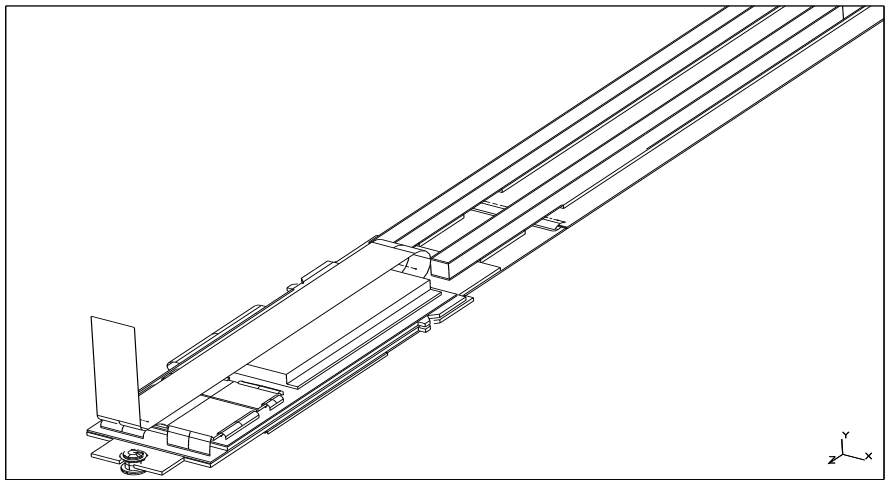

Figure 2: Perspective view of the ϕ-side of a Layer 0 ladder.

3 Sensor Research and Development

Severe constraints are placed on the design of the sensors for the SVX II detectors due to the radiation level and the short integration time for the read out electronics. Most of our research and development concentrated on the study of the double metal technology since it requires more challenging processing. Furthermore, the double metal layers 0 and 1 are closer to the interaction region and therefore have to sustain a larger radiation dose.

Type	Manufacturer	P-Side Implant Pitch (μm)	P-Side Readout Pitch (μm)	N-side Implant Pitch (μm)	N-side Readout Pitch (μm)
A	Micron/SI	25	50	103	103
B	Micron/SI	50	50	103	103
C	Micron/SI	50	50	80	160
D	Micron/SI	50	50	160	160
Delphi	Hamamatsu	50	50	42	84
L0	Hamamatsu	60	60	42	145
L1	Hamamatsu	60	60	42	133

Table 2: Prototype sensor geometry.

We incorporated into the design of the SVX II prototype sensors all characteristics currently known to be effective in minimizing radiation damage. This led to a biasing scheme with polysilicon resistors and to p^+ implants (p-stops) to provide isolation between the n^+-type strips due to the presence of an electron accumulation layer. The p-stops design used in the prototype development is shown in Figure 3. This isolation scheme is often called common p-stops since all p-stops are connected. We used wide p-stops which filled most of the region between the n^+ strips. On both sides, the strips were coupled to the readout electronics through an integrated coupling capacitor formed by a thin insulating layer and an aluminum electrode, often called the AC coupling electrode. The aluminum readout strip was stepped back by a couple of microns from the edge of

the implant in order to avoid discharges [2]. The prototype detectors were made with 300 μm thick n-type high resistivity bulk silicon.

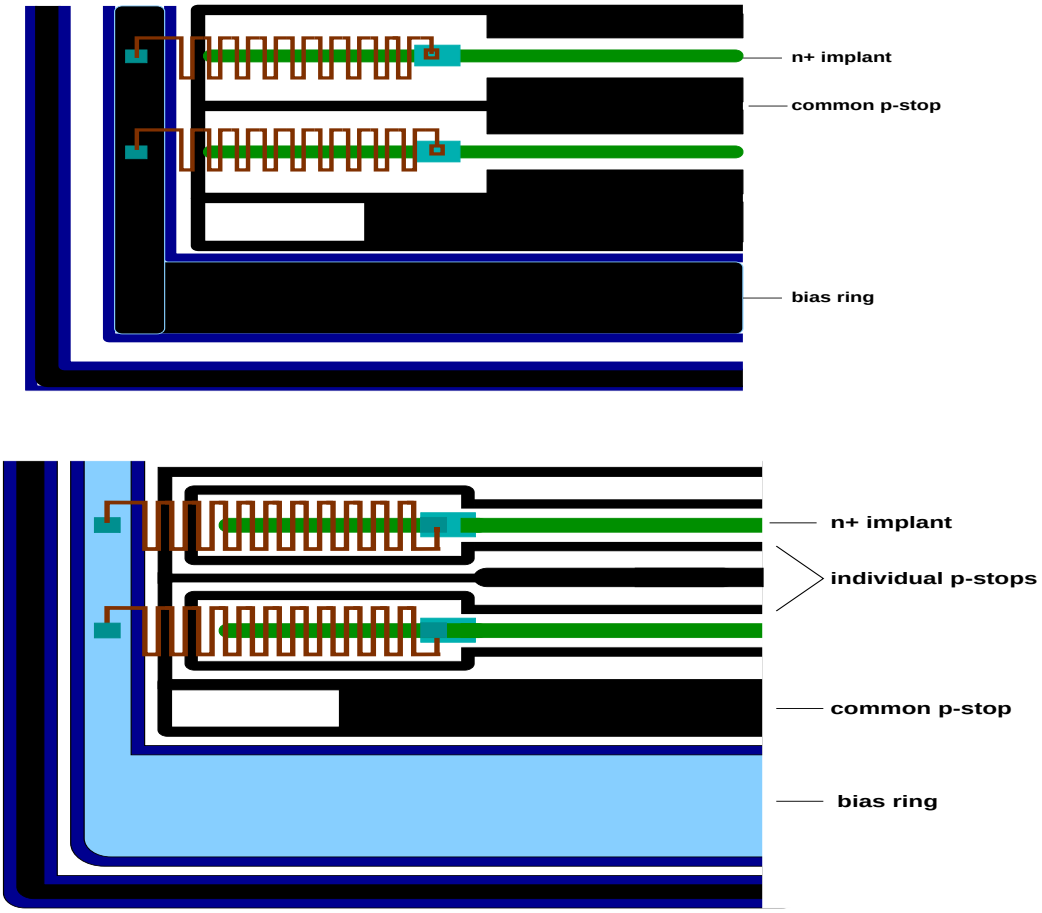

Figure 3: Layout of (top) common and (bottom) combined p-stops

The research and development for the silicon sensors included the investigation of several sensor geometries and different manufacturing technologies. The prototype detectors were manufactured by Micron Semiconductors, Sintef/SI and Hamamatsu Photonics. The readout and implant strip pitches for the prototypes are shown in Table 2.

Detectors of type C, D and L0 were layer 0 prototypes while A and B and L1 were layer 1 prototypes. A and B were half size

prototypes about 4 cm long. B and D had intermediate strips on the p and n side respectively. Each n-side readout strip is connected to $m \times g$ metal-1 strips, where m is the multiplexing factor and g is the ganging. Ganging is the number of neighboring n-side metal-1 strips connected to the same readout strip, while multiplexing is how many times that set of ganged neighboring strips is connected to the readout strip. The layout of one of our detectors with ganging of 2 and multiplexing of 2 is shown in top part of Figure 4.

3.1 Capacitance Minimization

The RMS noise of the SVX 2 chip versus input capacitance for integration times of 107 ns and 371 ns is shown in Figure 5. Using a linear extrapolation between the measured data points an input capacitance of 25 pF predicts noise values of $\approx$2100 e^- and $\approx$1100 e^- for integration times of 107 ns and 371 ns, respectively. Since two sensors are daisy chained to one SVX 2 chip, this requires the capacitance of each sensor to be less than 12.5 pF to guarantee a S/N larger than 12/1 at the beginning of operation. The average measurement of the n-side capacitance [3] of the prototype sensors is given in Table 3.

Sensor type	SI/Sintef	Micron	Hamamatsu
Layer 0	12.5	17.6	16.9
Layer 1	16.6	20.0	17.9

Table 3: Total n-side sensor capacitance in pF measured at 1 MHz.

The results show that all prototype sensors were close to or exceeded our goal of a sensor capacitance smaller than 12.5 pF. The SI/Sintef sensors show a lower capacitance since the double metal contribution is minimized by using polymide rather than SiO_2 as the insulator between the first and second metal layers.

The large n-side capacitance of the prototype sensors caused a major re-design of the double metal sensors. Several steps were taken to reduce the capacitance of the double metal sensors.

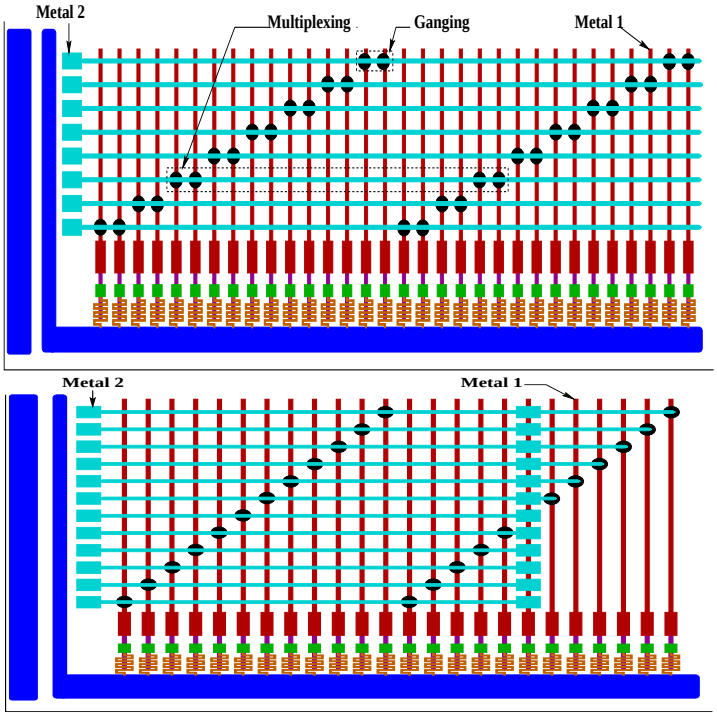

Figure 4: Layout of prototype (top) and production sensors (bottom).

The capacitance due to the double metal readout was minimized by making the SiO_2 between the two metal layers as thick as possible while maintaining the via reliability. SiO_2 was chosen as the insulator because of fabrication reliability and good radiation resistance. Also, the second metal line will be as short as possible. As shown in the bottom part of Figure 4, the metal will extend only from the bonding pads for the chip to the bonding pads for daisy chaining to the other sensor in the ladder. A new idea for the isolation p-stop pattern was introduced, in which a combination of an individual p-stop and a common p-stop is used. The combined p-stop design[4] shown in the bottom part of Figure 3 is expected to give a smaller n-side interstrip capacitance since two nearby n^+ strips are now connected by several capacitors in series. The average n-side capacitance expected for layer 0 and 1 sensors is about 10 pF

for the new design.

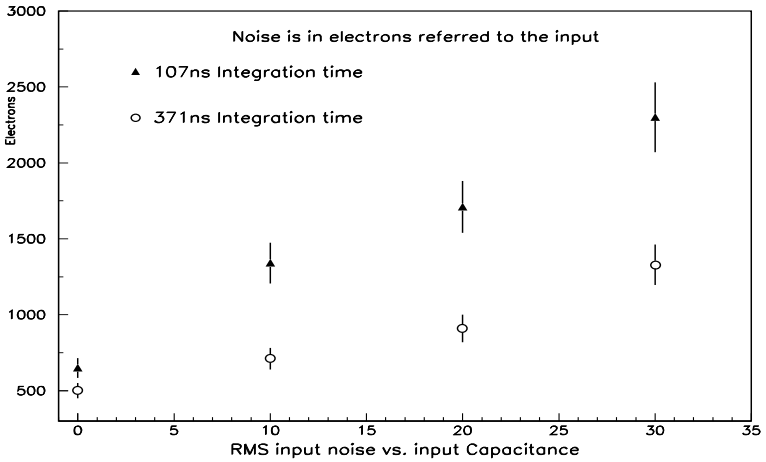

Figure 5: SVX2 measured noise as a function of input capacitance for integrations times of 107 ns (triangles) and 371 ns (circles).

3.2 Radiation hardness studies

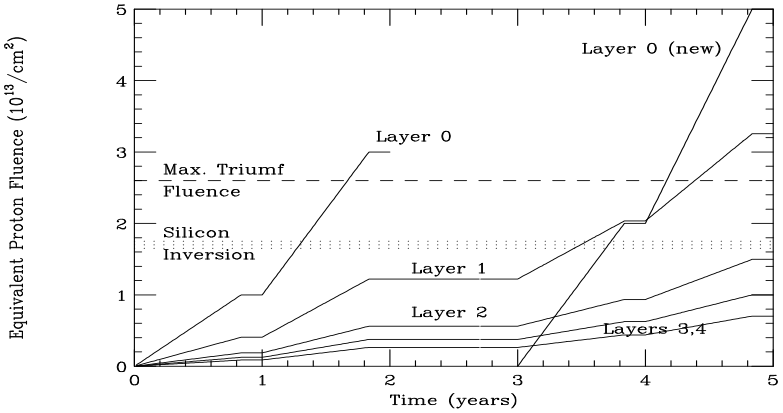

Figure 6: Estimated radiation levels for Layers 0-4 of SVX II in Run II.

We have studied the expected radiation dose for the SVX II as a function of time [5]assuming the integrated luminosity to be $1 f\mathrm{b}^{-1}$ and $2 f\mathrm{b}^{-1}$ for years 1 and 2, then 0 $f\mathrm{b}^{-1}$ for year 3, followed by

2 $f\mathrm{b}^{-1}$ and 3 $f\mathrm{b}^{-1}$ for years 4 and 5. We also make the assumption that Layer 0 will be replaced during year 3. The radiation dose is given as the equivalent fluence of 500 MeV protons[5]. As shown in Figure 6, the maximum fluence expected for the sensors is $\sim$ 0.9 Mrad and it is likely that during run II the SVX II will operate with the layer 0 sensors inverted.

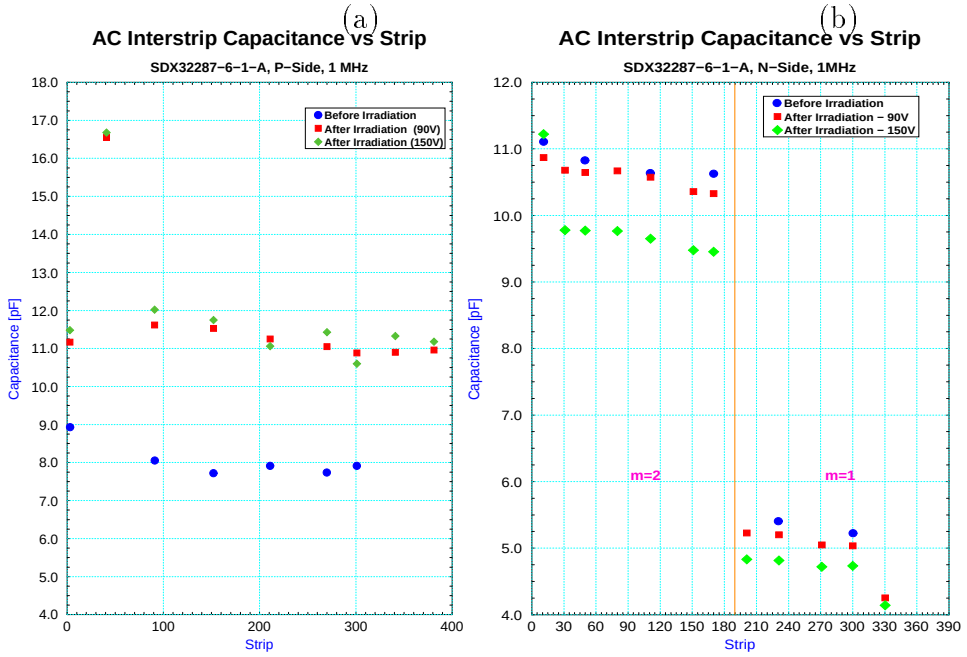

Figure 7: Measurement of (a) the p-side and (b) the n-side interstrip capacitance before and after irradiation.

We have extensively studied the SVX II prototype sensors from Hamamatsu, Micron and SINTEF/SI before and after irradiation at TRIUMF and at the Fermilab Booster. The TRIUMF and the Booster beam consisted of 400 MeV kinetic energy protons and 8 GeV protons respectively. The maximum proton fluence was about $3 \times 10^{13}/\mathrm{cm}^2$. In the case of the Booster run the radiation was very uniform. This was obtained by moving the detector on a precise x-y table. The TRIUMF run was known to have given non-uniform irradiation. The results show [6] no change in the value of the bias resistance and the coupling capacitance. The n-side interstrip resistance decreased from values above 2-10 GΩ before irradiation to

about 500 MΩ after irradiation. Nonetheless, the value of the interstrip resistance remains large enough that the sensor performance is not expected to be compromised.

Several other features of the silicon microstrip sensors show significant changes with radiation. These include the detector leakage current, the depletion voltage, and the interstrip capacitance. The change in the sensor interstrip capacitance is a result of surface damage caused by radiation at or near the silicon-SiO_2 interface. For the detectors uniformly irradiated at the Booster to about 1 Mrad (passing the n-type to p-type inversion point), we observe an increase of 40 % in the sensor p-side interstrip capacitance. The n-side interstrip capacitance remains unchanged or decreases by about 10%. The value of the n-side interstrip capacitance depends on the bias voltage. The results are shown in Figure 7. Similar measurement by groups working towards the development of detectors for the SSC [8] and the LHC [7] are in agreement with our findings.

3.3 Integrity of the coupling capacitors

In order to reduce the impact of leakage current increase due to radiation damage, silicon microstrips are often connected to the readout electronics through a coupling capacitor which is integrated into the sensor by depositing a thin dielectric between the implant and the aluminum readout strips. Such a detector is referred to as an AC coupled detector. Robust and reliable AC coupled detectors are required for tracking at high luminosity hadron colliders. A broken capacitor will allow excessive current to enter the readout chip and can spread across several channels. This can lead to what is called a black hole and can render several channels unsuitable for particle tracking. Since irradiation increases the sensor depletion voltage and full efficiency is achieved only by over-depletion, SVX II is planning to adopt a split bias scheme so that the coupling capacitors on each side of the sensor will be required to hold only half of the bias voltage. We expect to operate the readout electronics at ground.

We detect defects in the coupling capacitors by applying a voltage across the coupling capacitor and measuring the current. Hamamatsu detectors have an aluminum "proving pad" on each end of the detector which directly contacts the n-type bulk silicon. In order to

check the integrity of the coupling capacitor on the p-side (n-side), we connect the proving pad to ground and apply a positive (negative) voltage to the AC pad. In the case of a good capacitor, no current will flow since the voltage drop will be across the coupling capacitor. In contrast, if the capacitor is damaged, the implant will be at the same potential as the aluminum strip and the junction will be forward biased, allowing a current to flow.

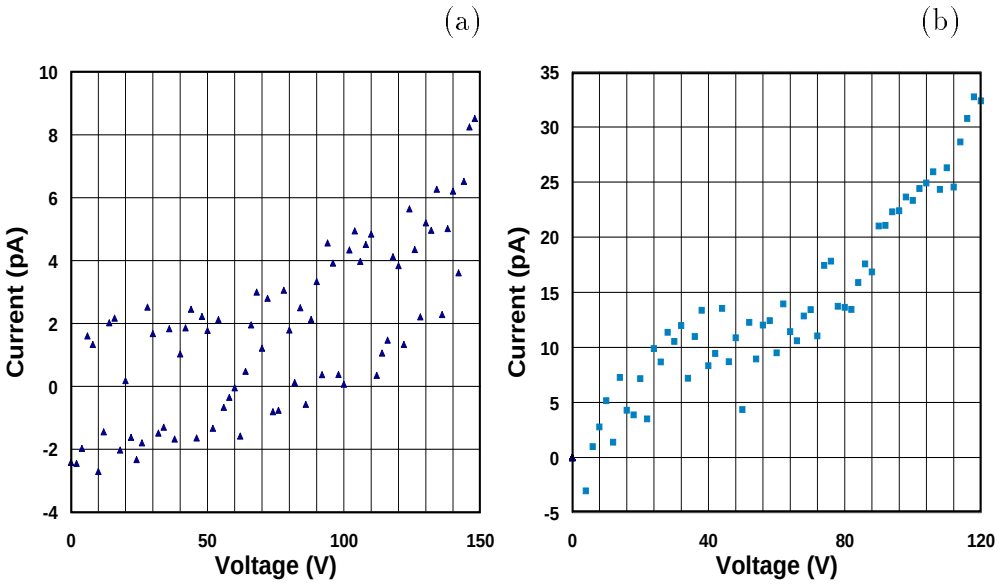

Figure 8: Current versus voltage (a) before and (b) after irradiation.

In order to understand the mechanism yielding the observed defect in the coupling capacitor, we studied the behavior of strip breakdown as a function of voltage. In Figure 8a we show the current as a function of the voltage for a good strip from detector SDX33181-17-0. The current oscillates between $+2pA$ and $-2pA$ up to approximately $70V$. Above $70V$, the current increases with voltage but never rises above the current limit. The fluctuations in the current are consistent with surface effects and noise in the measurement system.

We find two different breakdown behaviors. The first type yields what is considered a pinhole, defined as a direct connection between the implant and the readout strip through the SiO_2. Pinholes allow

current to flow to the chip as soon as a potential difference is applied between the implant and the aluminum readout strip. In this case, the strip draws a current $\geq I_{thresh}$, usually at the first applied voltage.

The second type of breakdown is an increase in the current as shown in Figure 9a which increases the noise on the strip. These defects are called microdischarges and are due to localized and reversible breakdown of the bulk silicon near the implant strips. Microdischarges have been studied extensively in [2],[9],[10]. In general, microdischarge should only appear at high voltages when the electric field in the bulk near the strip is large. Microdischarges are found mainly on the p-side, in agreement with a numerical calculation [2, 9, 10] that predicts the E field near the p-side implants to be larger than on the n-side.

3.4 Radiation effect on the coupling capacitors

In order to study the effects of irradiation on the SVXII detectors, tests to detect defects on the coupling capacitors are run both before and after irradiation. Detector SDX32287-6-1A received a uniform dose of $\sim$ 1 Mrad at the Fermilab booster with 8 GeV protons. A good strip on the irradiated detector SDX32287-6-1A is shown in Figure 8b. We notice that the measured current after irradiation is always larger than zero in contrast to the result before irradiation. This is consistent with an increase in surface current due to the irradiation.

We find more defects in the coupling capacitors after irradiation. Six more strips on the n-side are consistent with pinholes and two more on the p-side break down at high voltages. This is a 1.6% increase of defects on the n-side and a 0.5% increase on the p-side. Also, we observe a decrease of the breakdown voltage after irradiation. In fact, the breakdown voltages are larger than $120V$ for the non-irradiated sensor and less than $100V$ for the irradiated sensor. The current as a function of the voltage for one of the strips showing microdischarge is shown in Figure 9b.

Several changes are planned by Hamamatsu[2] for the production detectors in order to increase the onset voltage of microdischarge, such as a geometry in which the SiO_2 overhangs the implant. In this case, the highest field is pushed inside the SiO_2, which has a

field breakdown about 30 times higher than bulk silicon. The new design also uses a thicker insulator which combines layers of SiO_2 and SiN_3. Nonetheless, the issue of the integrity of the coupling capacitor after irradiation requires further studies.

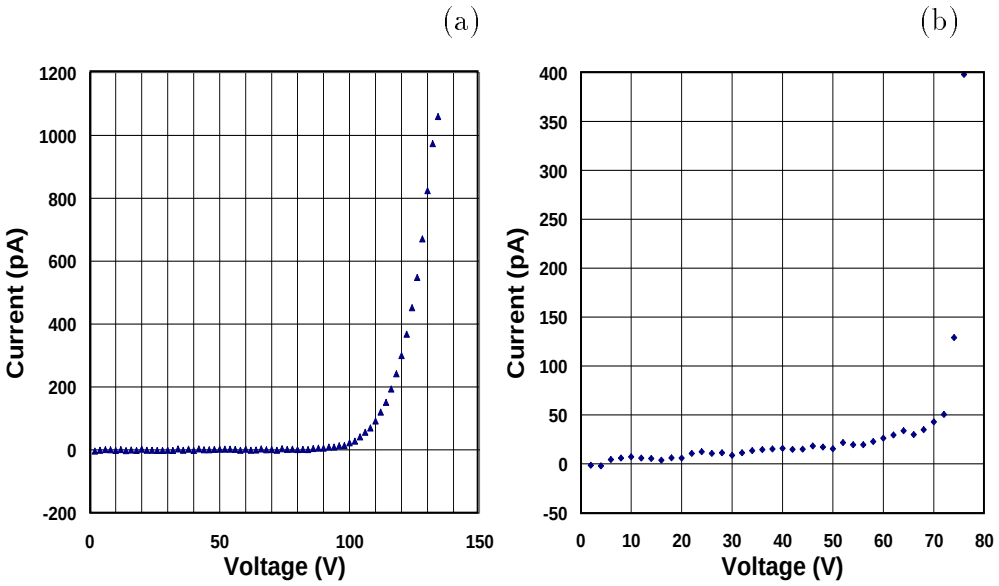

Figure 9: Breakdown behaviour (a) before and (b) after irradiation irradiation.

3.5 Beam tests

Two beam tests were carried out with the prototype detectors to study different clustering algorithms, the n-side resolution versus incident track angle, the p-side performance after inversion and the signal to noise (S/N) dependence on bias voltage. The principle difference between the two beam tests at KEK was the type of chip used to read out the sensors. In the first beam test[11] the well-understood SVXH chip was used, while in the second test[12] the prototype SVX2 chip was used.

In the first KEK beam test, five (SINTEF/SI and Hamamatsu) double-metal detectors were tested. The position resolution of these detectors as a function of angle is shown in Figure 10. At normal

incidence the strip pitch/$\sqrt{12}$ accounts for the resolution. For particles with oblique incident angles the resolution varies between 12 and 25 microns.

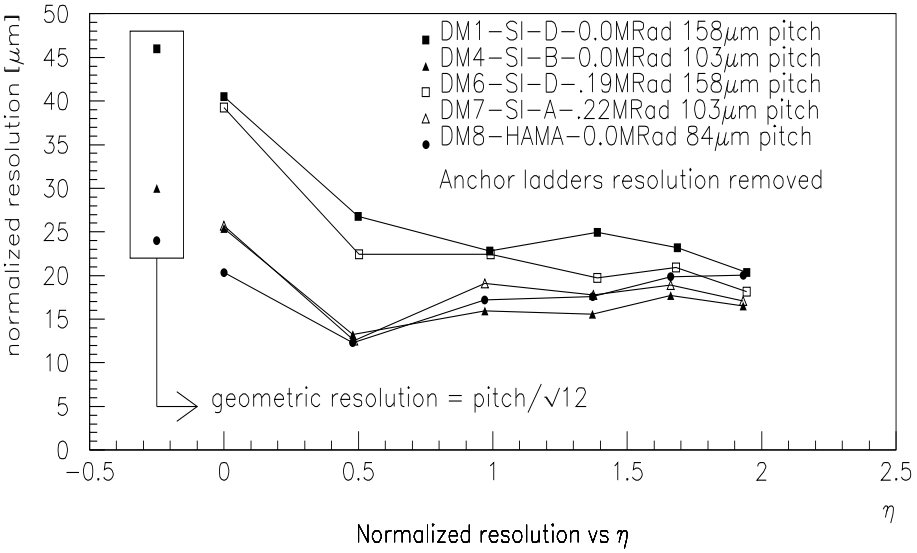

Figure 10: Position resolution versus incidence angle

The S/N of irradiated and unirradiated SVX II prototype sensors was measured in the two beam tests at KEK. In the first KEK run, the unirradiated detectors have an n-side S/N ratio between 16 and 21, while detectors irradiated with 0.25 and 1.0 Mrad have S/N ratios of 13 and 14. In the second KEK beam test, S/N ratios were measured for seven double-metal detectors supplied by SINTEF/SI, Hamamatsu, and Micron. Unirradiated detectors have ratios between 11 and 14, while irradiated detectors, having doses between 0.1 and 0.7 Mrad, have ratios between 7 and 10.

The S/N measured during the second test beam is somewhat lower due to several effects. The dominant effect is from the increased noise of the SVX2 chip as operated for the KEK test, i.e. there was excess noise beyond what can be expected for optimized running conditions. Furthermore for some runs there was a loss of signal up to 14 % because of lack of synchronization between the

chip integration and the KEK trigger window [13]. The noise as a function of average radiation dose is plotted for the p-side in Figure 11 and for the n-side in Figure 12. The p-side detectors had strips of two different lengths, 4.1 and 8.2 cm. The results for these are plotted separately. Whereas the n-side shows no evidence for an increase of noise with radiation dose, the p-side shows an increase. For the p-side, the solid lines in Figure 11 indicate a range of expected noise as a function of dose assuming that the inter-strip capacitance increases between 20% and 40%. We find good agreement with our expectations for the short detectors. The long detectors show a smaller noise increase than expected because of the non-uniform irradiation. Efforts are continuing to understand the S/N and to decrease the chip noise.

4 Conclusions

The SVX II detector is expected to be operational in 1999. Sensor delivery, ladder construction and the final design of the SVX 3 chip are on the critical path for the completion of this project. An extensive program of research and development of double sided double metal silicon sensors has resulted in a major redesign of our production detectors. We have found some evidence of an increase in the defects of the integrated coupling capacitors after irradiation which will require further investigation.

The signal to noise ratio obtained in the KEK test beam lead us to believe that we can meet the requirement for run II. We are working to further reduce the noise of the SVX 3 chip at the higher 53 MHz bandwidth.

5 ACKNOWLEDGEMENTS

I would like to acknowledge the help of the SVX II design group. Special thanks also to the organizing committee for the impeccable setting and the gorgeous weather.

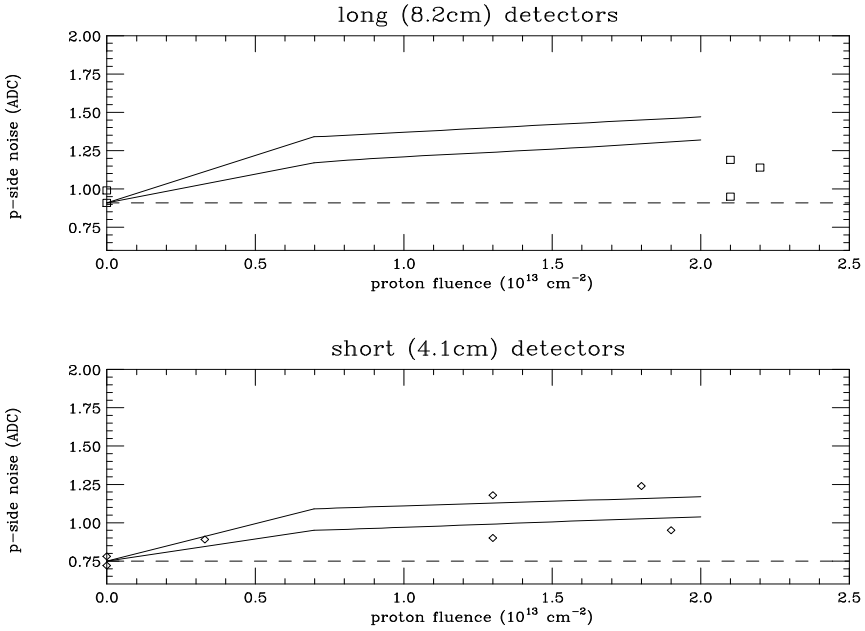

Figure 11: p-side noise versus average radiation dose for the 5 long and 7 short detectors. The solid lines in the figures indicate a range of expected noise as a function of dose. The dotted line indicates the average unirradiated noise value. None of the detectors were believed to have been inverted at the time of the measurements.

References

[1] S. Kleinfelder, *et al.*, A flexible 128 channel silicon microstrip detector integrated circuit with sparse data readout, IEEE Trans. Nucl. Sci., Vol. 35, No.1, 171 (1988). R. Yarema, *et al.*, A Beginner's Guide to the SVX II, FERMILAB-TM-1892.

[2] T. Ohsugi *et al.*, Nucl. Instr. and Meth. A 342 (1994) 23.

[3] D. Bortoletto, *et al.,* Capacitance measurement of double metal double sided silicon microstrip detector, Proc. Second International Symposium on Development and Application of Semiconductor Tracking Detectors, Hiroshima, 1995, to be published in Nucl. Inst. and Meth. A. M. A. Frautschi, *et al.,* Capac-

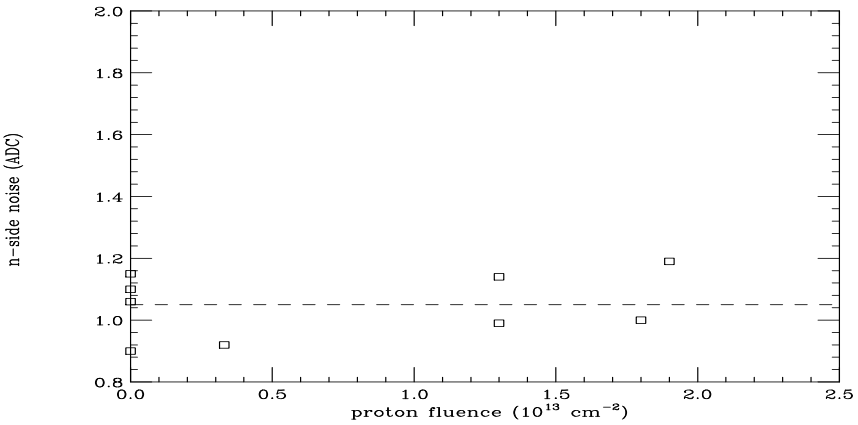

Figure 12: n-side noise versus radiation dose. The dotted line indicates the average unirradiated noise value. The irradiated n-side results are all of the short variety. None of the detectors were believed to have been inverted at the time of the measurements.

itance Measurements of Double-sided Silicon Microstrip Detectors, FERMILAB-PUB-96/008-E, submitted to Nucl. Instr. and Meth. A.

[4] This new design was developed by T. Ohsugi in collaboration with Hamamatsu.

[5] J. Matthews *et al.,* Bulk Radiation Damage in Silicon Detectors and Implications for SVX II, CDF Note 3408 (1995).

[6] D. Bortoletto, *et al.,* Irradiated SVX II prototype probing results, CDF/DOC/SEC_VTX/CDFR/3295.

[7] RD20 Collaboration, A. Holmes-Siedle *et al.,* Radiation Tolerance of Single Sided Silicon Microstrips, CERN-PPE/93-137 (1993).

[8] Y. Unno *et al.,* Characterization of an Irradiated Double-sided Silicon Strip Detector with Fast Binary Readout Electronics in a Pion Beam, IEEE 1995 Nuclear Science Symposium, San Francisco, CA Oct 25, 1995, KEK Preprint 95-172 (1995).

[9] T. Ohsugi *et al.*, HUPD 9507, to be published in Nucl. Instr. and Meth. A.

[10] T. Ohsugi *et al.*, HUPD 9508, to be published in Nucl. Instr. and Meth. A.

[11] N. Bacchetta, *et al.*, Resolution of Double-Sided Silicon Microstrip Sensors, CDF/DOC/TRACKING/PUBLIC/3277.

[12] N. Bacchetta, *et al.*, Results of the KEK Beam Test of SVX II Prototype Detectors, CDF/DOC/TRACKING/PUBLIC/3547.

[13] C. Gay *et al.,* Anatomy of the SVX II Pipeline and the KEK Beam Test Signal-to-Noise, CDF Note 3514 (1995).